Chapter 7: Error Analysis

We now list the sources of error which could affect our measurements and the resulting error level of each. These include

1. uncertainty in the correct value of σ_0 for the beam, resulting both from energy and quadrupole calibration errors and from the nonlinearity of the focusing field.
2. omission of part of the beam from measurement,
3. longitudinal space-charge effects near the ends of the beam,
4. non-zero slit-size corrections,
5. slit misalignments with the quadrupole symmetry planes,
6. space-charge forces in the drift region between slits,
7. space-charge perturbations due to the presence of the slits in the beam,
8. pulse-to-pulse variation of the beam,
9. background gas collisions with beam ions, and
10. secondary electron yield variations.

We will examine each of these possible sources of error, estimating bounds for each, and at the end of this chapter will summarize the results.

7.1 Errors in determination of σ_0

We have determined the beam energy to be 122.5 ± 1 keV, and we know the quadrupole voltage to within about $\pm 0.4\%$. The relative uncertainty of about 1% between the beam energy and quadrupole voltage results in an uncertainty in the value of σ_0 for paraxial particles of about 0.5% near $\sigma_0 = 60°$,

increasing to about 1.3% near $\sigma_0 = 140°$. In addition to this error, there is an uncertainty in the appropriate value for σ_0 because of the lattice nonlinearity. In order to estimate this uncertainty, we used the envelope equations to calculate the matched beam size in the SBTE lattice using the measured values of quadrupole voltage, emittance, and current. The maximum beam radii were all at least 10 mm within the focusing lenses. We then calculated σ_0 for single particles attaining a 10 mm maximum displacement. The values of σ_0 for paraxial particles calculated for a 1% relative error between the particle energy and the quadrupole voltage, making the lattice weaker, and those calculated for the voltage error in the opposite direction for particles attaining a 10 mm maximum excursion have been taken as the limits of uncertainty in the σ_0 value characterizing the lattice. More information on the nonlinearity of the lattice is given in Appendix D.

7.2 Incomplete scans of phase space

We compared the total beam current calculated from the phase space measurements against the current as measured by the various Faraday cups to ensure that we had sampled the entire beam. The sum of the phase space measurements should be proportional to the total beam current, as follows. We denote the upstream and downstream slit widths by w_1 and w_2, respectively, and the scan increments by Δ_1 and Δ_2. During the measurements, only w_1/Δ_1 of the beam particles will pass the first slit, and only w_2/Δ_2 of these will pass through the second slit into the detector. If ξ is the overall gain of the detector and R is the resistance used as the oscilloscope termination, then

$$\sum_{i,j} f(x_i, x'_j) = \xi \frac{w_1}{\Delta_1} \frac{w_2}{\Delta_2} IR. \tag{7.1}$$

where the values $f(x, x')$ are the measured signals. The intercalibration of the proportionality constants was done with the constant-current, $\sigma_0 = 60°$, beam conditions used for cup calibration.

We calculated the intercepted current for each set of beam parameters subsequently used, and compared the values obtained with Faraday cup current measurements made along the lattice. In some cases, we failed to make the mid-lattice cup measurements, and have only the value of the current calculated from the emittance measurements. Because the cup-measured current and the current calculated from the slit measurements differ by 10–20% for most of the $\sigma_0 > 118°$ beam measurements, there is an additional uncertainty in the values of beam current along the lattice for beams undergoing current loss. (That this lower current was not due to failure to scan over some of the beam-occupied phase space was shown by subsequent scans made over a much wider phase space area. The subsequent scans showed the same intercepted beam current as the first scans.)

There are two possible causes for the discrepancy. The first is that the beam may have been surrounded by a diffuse cloud of ions, driven from the beam by either collective interactions or the emittance grids, and having too low a density to be picked up distinctly by our diagnostics. We do not believe this to be the case, because the missing current would give an observable signal if spread out over the entire lattice acceptance. For $\sigma_0 \sim 130°$, the zero-current acceptance of the lattice (allowing particles to take up the entire 25.4 mm bore radius) is about $1 \times 10^{-3}\pi$ meter radian, unnormalized. Each two-slit sample point with 0.01-inch slits at a 6-inch spacing covers about $1.4 \times 10^{-7}\pi$ meter radian, or about 1.4×10^{-4} of the total acceptance. If a typical "missing" beam current of 1 mA were spread out equally over the total lattice acceptance, there would be a background signal of at least .8

mV, or (1 mA) $\times$ (1.4×10^{-4}) $\times$ (500 Ω) $\times$ 12 (the secondary emission gain factor). Because misalignments restrict the available bore by several mm at this lattice strength, and because the missing current would have to be in the phase space not sampled in the measurements, the background level required to account for the 1 mA is really about 2 mV, well above the observed noise level of about $\pm$0.4 mV.

We thus conclude that the most likely cause is the high divergence of the beam at high σ_0. Most of the scans for $\sigma_0 > 118°$ were made in the convergent beam dimension. The source of the discrepancy with cup current measurements lies in the high divergence of the beam in the other plane. With the quadrupole between the first and second measurement slits grounded, some of the particles can lie outside of the acceptance of the slits, not in the plane of the measurement (say, the x plane), but in the plane of the slits. See Fig. 7.1 for a graphic illustration of this effect. The quadrupole between the two slits must be grounded to make the measurement of x'. If the beam divergence is marginally too large to allow the beamlet to fall entirely within the limits of the slit, then any misalignment or mismatch of the beam can cause part of the beam to miss the slit. Because of the linear optics and generally elliptical cross-section of the beam, particles with very large values of y' have associated large displacements in y, and they tend to have small offsets in x. If some of these particles were lost while measuring the phase space distribution in the x dimension, the $f(x, x')$ signals would have been clipped near small x, where they are at their maximum. One can recover the correct measurement of phase area, but not the emittance ellipse shape and orientation, by turning the strength of the quadrupole just upstream of the primary slits to about one-half of its nominal value. In effect, this converts a highly divergent beam into a roughly parallel beam and allows the current to be directed into the area covered by the slit cups. We chose to leave the

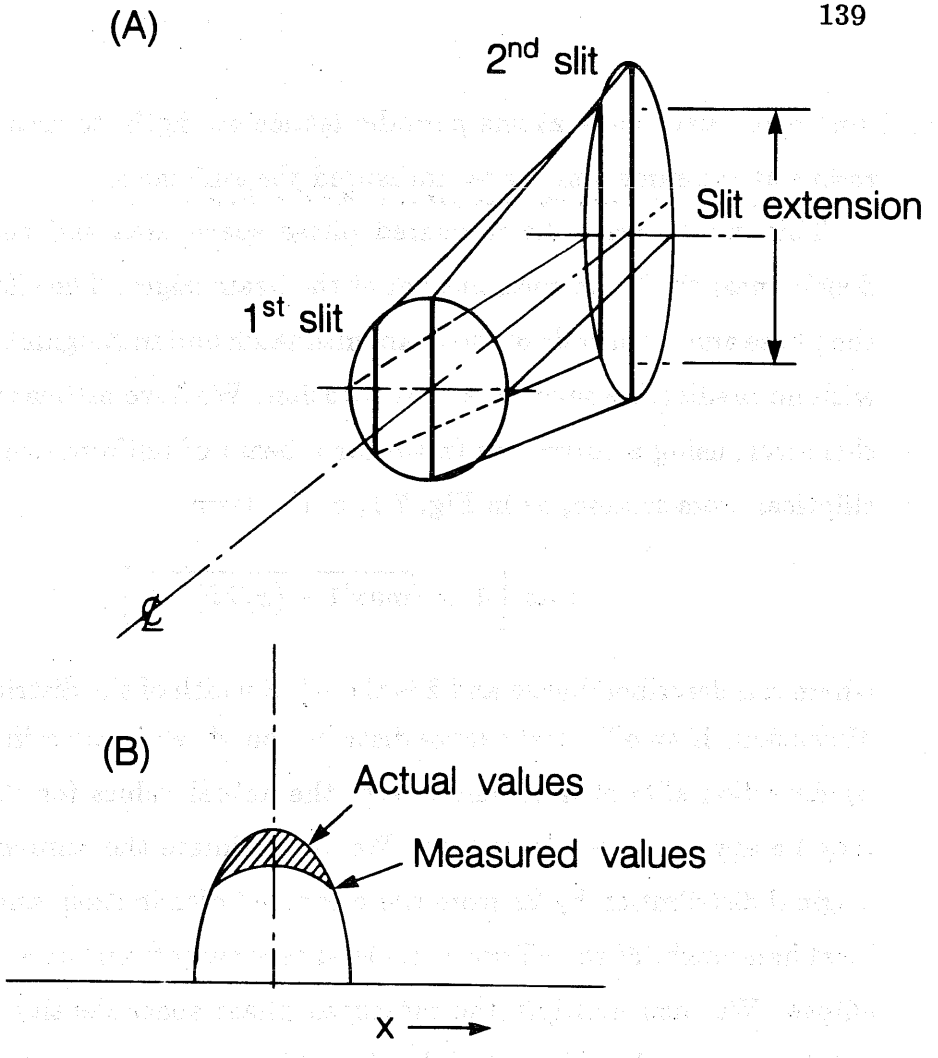

XBL 863-10351

Figure 7.1: When the beam is convergent in the plane perpendicular to the slits, the effect of the non-zero width of the first slit is minimized, as shown in section 7.4. The beam will not fall outside the measurement acceptance in the plane of the measurement. However, if the beamlet overfills the downstream slit in the divergent dimension, part of the current will be lost, causing too low a value for the phase space density at that (x, x') point. The affected data tend to be near the center of the beam in the x dimension, where the density is greatest. The RMS emittance calculated from the measured distribution will be too large, as a result. For our measurements, this error is estimated to be in the range 0–10%.

upstream quadrupole at the periodic lattice strength, to measure the beam radius at the same time as we measured the emittance.

This error lowers the measured phase space area and the phase space density near the beam core, but not at the beam edges. The effect depends on the phase and amplitude of the beam mismatch and misalignment oscillations, with no predictable severity at any location. We have estimated the effect of this error, using a correction factor for a beam of uniform density beam and elliptical cross-section, as in Fig. 7.1, of the form

$$\max\left[\,1, \alpha\sqrt{\max[1-(x/2\tilde{x})^2, 0]}\,\right], \tag{7.2}$$

where α is described below and $\tilde{x}$ is the RMS width of the distribution in the x dimension. If an elliptical charge distribution of semi-axis α in y is truncated by detection slits of unit half-length, the actual values for the distribution may be approximated as follows. We approximate the semi-axis in x of the original distribution by $2\tilde{x}$ from the measured distribution, and calculate the local half-height of the ellipse at a distance x away from the x-centroid of the ellipse. We then multiply the measured phase space density values at that point in x by the local height of the ellipse if it is greater than 1. For $\alpha \leq 1$, the distribution is unaltered. As the value of α is raised, the total current in the corrected distribution rises, with values of the phase space density near the beam center raised preferentially. If the measured width of the distribution is close to the true width and the data are of the form assumed in Fig. 7.1, then the actual distribution in phase space is recovered for α chosen so that the corrected total current agrees with the Faraday cup measurements. Analysis of the corrected data yields marginally smaller emittance values than for the raw data, but the difference is no more than about 7% for ϵ_{95} and ϵ_{100}. Thus the data are reliable, and we are able to place narrow bounds on the error from this mechanism in calculating the emittance of the beam. Although the

beam sizes and divergences calculated from the envelope equations do not indicate that the beam should overfill the emittance scan slits as suggested above, beam misalignment could have allowed the beamlets to spill over one end of the downstream slit.

7.3 Beam end-effects

Our measurements were made near the center of a 10 μsec-long beam pulse (physical length about 4 meters). The beam rise and fall times at the ends are a fraction of a microsecond at the beginning of the transport system and degrade (because of longitudinal space-charge effects) to about 2–3 μsec at the end of the channel. Hence the measurements we report are representative of an infinitely long beam. The development of local debunching at the beam ends along the lattice is apparent in Fig. 5.3. Control of the bunch ends is a separate research effort beyond the scope of this thesis.

7.4 Effect of non-zero slit size

We have calculated the effect on the emittance measurement due to the use of slits of non-zero width. The result (for a linearly focused beam) for the mean square width of a beamlet passing through a primary slit at $z = 0$ and measured a distance L downstream, is

$$\langle x^2 \rangle_{z=L} = L^2 \tilde{\Theta}^2 + m^2 \frac{a^2}{12} + \frac{b^2}{12}, \tag{7.3}$$

where $\tilde{\Theta}$ is the local RMS angular width of the beam distribution at the first slit, m is a magnification factor to be defined shortly, a is the full width of the first slit, and b is the full width of the second slit. To see this, we write the position and angular dependence of the beam distribution at the upstream slit in the form $f(x,p)$, where $p = x' - sx$ and $s = -1/f$. The parameter s describes the focusing of the beam in terms of the distance f to the geometric

focus of the beam. The distance f is positive for a convergent beam and negative for a divergent beam. This parameterization is used to separate the convergence of the beam from any other spatial or angular dependence. We will consider in detail only the effects of the non-zero size of the first slit. The second slit may be accounted for in a similar fashion.

A particle with coördinates (x, x') at $z = 0$ will have coördinates $(x + Lx', x')$ at $z = L$, so

$$\langle x^2 \rangle_{z=L} = \langle (x + Lx')^2 \rangle_{z=0} = \langle (mx + Lp)^2 \rangle_{z=0},$$

where $m = 1 + sL$ is the geometric size of the primary slit projected onto $z = L$ by the beam. For a beam distribution even in p, the cross term xp averages to 0, and the mean square beamlet size at $z = L$ reduces to averages of x^2 and p^2 over the collimated beam distribution at the first slit. We will write the slit distribution as $g(x)$, so that the collimated distribution of the beamlet at $z = 0$ is $f(x, p)g(x)$. If we assume that the first slit is very narrow, then the collimated distribution may be written as the product of a purely angular dependence from the beam (apart from the focusing) and a spatial dependence from the slit, as

$$f(x, p)g(x) \sim F(p)g(x),$$

where F describes the angular distribution of the beam at the center of the slit. The averages then reduce to the form quoted in Eqn. 7.3. The higher-order corrections due to the variation of f with position within the slit (apart from convergence, which we have handled properly) are of the order of the square of the ratio of the slit size to the beam diameter ($\sim 10^{-4}$ in our case, considered negligible). In the instance of a convergent beam, the effect of the nonzero size of the first slit disappears for $m = 0$. This error contributes to an

overestimate of the emittance and was checked by comparing measurements for the convergent and divergent planes for many of the beam configurations for $\sigma_0 < 100°$. We saw no difference in emittance between the two planes of more than a few percent, except for the intentional asymmetry in emittance introduced for the measurements of section 6.1.

7.5 Slit misalignment

Slit misalignments with the each other and with the quadrupole symmetry planes increase the effective size of the slits. The alignment procedure used on SBTE relied on optical alignment of the slits with the same cross-hairs in a transit telescope that were used to set up the quadrupoles themselves. Slit parallelism was further checked by shining a light through both slits and checking the uniformity of illumination through the pair of slits with the telescope. The estimated misalignment between the ends of the 2 in-long slits was less than 0.005 in, making the effective width of the beam-occupied portion of the slit at most 0.013 in. We included the effects of misalignment by using this allowance for the size of the slits.

7.6 Space charge effects

We have estimated the space-charge effects by integration of the envelope equations for the beamlet passed by the upstream slit. We included the overall convergence and divergence of the beam, using twice the RMS radius of the slit as the initial radius in one dimension, and twice the RMS radius of the beam as the beamlet radius in the other dimension. The current transmitted through a slit at the beam centroid was estimated from the phase space measurements, and the level of the error introduced by the space-charge was taken to be bounded by the ratio of the beamlet radius calculated in the presence of space-charge to the radius calculated for a zero-current beamlet. The correction varies from 1% to 4%, with the actual beam emittance smaller

than that calculated directly from the data.

An estimate for the correction may also be obtained by taking a zero-emittance model beam, and calculating the transverse field due to the space-charge of the slab beamlet transmitted through the first slit. For particles at the beamlet edge, the electric field may be taken as constant, apart from the convergence or divergence of the beam in the direction parallel to the slit, as

$$\mathrm{E}_{\perp} = \frac{\rho d}{2\epsilon_0}.$$

The space-charge deflection of the particles during the 6 in drift between slits may be easily calculated, and gives a bound on the error of a few percent in the beamlet size at the second slit, in agreement with the envelope equation calculations.

7.7 Slit-beam perturbation

Another effect on the beam related to space-charge forces alters the focusing properties of the beam near the first slit. The conducting slit shorts out the transverse self-field of the beam for a distance of about one beam radius from the slit, causing the beam to be less divergent than it would have been in the absence of the slit. The result is less than a 0.1 mm shift in beam size and a few milliradian shift in convergence angle. For example, for $I = 15.2$ milliampere, $\sigma_0 = 83°$, and $R_{\mathrm{Beam}} = 0.012$ meter, we have a local transverse self-field of 50 kV/meter. This results in a change in beam radius on the order of 15 μm, or about 0.001 in. The change in divergence is more noticeable, giving $\Delta\theta \simeq 2.5$ milliradian at the beam edge, compared to a typical divergence angle at the beam edge of about 70 milliradian. This affects the emittance measurement only through the higher order effect of aberrations in the beam focusing, which we have considered to be negligible.

7.8 Pulse-to-pulse variation of the beam

Overall reproducibility was good on a long-term basis, with particular reference conditions at $\sigma_0 = 60°$ yielding reproducibility in total current intercepted in the two-slit scans and in the calculated RMS emittance at the 1% level over a period of months. However, for some of the $\sigma_o > 100°$ measurements, the variability was greater, resulting in values for the beam emittance estimated to be too large by as much as 6–8%. This estimate was made by interpolating and smoothing the most seriously affected data by hand and comparing the total emittances before and after the smoothing.

7.9 Background gas effects

Because the electrostatic quadrupoles sweep free static charges from the bore, space-charge neutralization is unimportant for SBTE. Beam-gas nuclear collisions are negligible, and electronic interactions cannot supply enough momentum exchange to deflect the Cs^+ ions by significant angles. The charge-state changing interactions of electron capture and second ionization are the only effects of the background gas on the beam. Neutralized cesium ions are lost to the beam, but under certain circumstances Cs^{+2} ions may be retained and be counted twice in the current monitors.

The measured cross-sections for these interactions in the SBTE imply that at normal operating pressures in the neighborhood of 5×10^{-7} Torr, only about 2% of the beam particles will undergo a charge-state changing interaction. See section 6.3 for the detailed measurements made with the SBTE. We found no effect on the beam emittance within the usual scatter of a few percent when we measured the emittance of the full-current, $\sigma_0 = 60°$, beam over the range of pressure 1×10^{-7}–2×10^{-6} Torr, although the beam current had been attenuated by charge-exchange interactions at the higher pressure by about 7%.

7.10 Secondary electron yield variations

Secondary electron yields may vary somewhat over a surface, depending, for instance, upon variations in adsorbed gas coverage. The slit cup collectors are very limited in actual area used, the maximum area being about 2 in by 0.08 in. The slit cups are probably immune to secondary yield variations other than a uniform variation over the surface as a function of time, which we believe to be small. The materials used are the same as for the SFC's, which showed no perceptible variation in response over the duration of the measurements, and we saw good agreement of the integrated slit cup current with the Faraday cup current measurements for $\sigma_0 < 100°$ throughout the experimental period.

7.11 Error summary

We have identified several (primarily systematic) sources of error. The amount of the error from each mechanism varies with the dominance of the space-charge in the beam. In plotting the i vs. $\epsilon(i)$ curves, as well as in the phase space contour curves, these errors have been ignored. However, in the quoted values of the emittances ϵ_{95} and ϵ_{100}, the systematic errors have been corrected. In Table 7.1 we have summarized the effect of these errors, and indicated the typical correction resulting from them. The effect of these emittance corrections is small in the derived σ_{100} and σ_{95} depressed phase advance values. The error in these values is due primarily to the noise in the tails of the phase space distribution data, and we believe that the value of σ representing the actual beam parameters lies within the bounds given by σ_{100} and σ_{95} in Fig. 5.11 and Table 5.1.

Mechanism	Error Bounds	Comments
Errors in lens voltage Intrinsic lens nonlinearity	$\pm 1°$ to $\pm 3°$	Calculated for paraxial partricles with 1% low lens strength and for 10 mm maximum orbit amplitude for 1% high lens strength
Collimating slits too short	0–7%	Makes measured values for ϵ too large, primarily for $\sigma_0 > 100°$
Nonzero slit size or misaligned slits	0.5–2%	Measured values for ϵ too large
Nonzero space-charge during drift between slits	0.7–4%	More severe for $\sigma_0 < 100°$
Variation between pulses during beam measurements	0–6%	Measured values for ϵ too large
Collisions of beam particles with background gas particles	$< 3\%$	Causes beam loss, with effect on ϵ dependent on retention of second-ionized particles. Major effect is 1–2% beam loss

Table 7.1: Summary of error bounds